ACOUSTICS 2012

Stochastic prediction of broadband shock-associated noise including propagation effects

C. Henry[a], C. Bailly[b] and G. Bodard[a]

[a]SNECMA, Rond-Point René Ravaud, Réau, 77550 Moissy-Cramayel, France
[b]Laboratoire de Mecanique des Fluides et d'Acoustique, 36 Av Guy de Collongue 69134 Ecully Cedex
cyprien.henry@snecma.fr

When operated at off-design conditions, supersonic jets produce BroadBand Shock-Associated Noise (BBSAN). The noise is generated by the interaction of the quasi-periodic shock-cell structure with the large scale turbulence. BBSAN radiation is characterized by multiple frequency humps dominating the jet mixing noise in the forward quadrant. A semi-analytical prediction method is presented in this paper. BBSAN sources are formally derived from the Linearized Euler Equations (LEE) and then numerically computed using a CFD calculation of the mean flow. A ray-tracing method is used to account for potential refraction effects, the outline of which is presented. The acoustic results are compared with experimental data to assess the model capabilities.

1 Introduction

During cruise-phase, engines of civil aircrafts are operated at high Nozzle Pressure Ratios (NPR), especially for the secondary stream. This results in a supersonic jet flow exiting from the aft of the secondary nozzle and producing supersonic jet noise.

Supersonic jet noise is created by the combination of three phenomena: mixing noise, screech tones and BroadBand Shock-Associated Noise (BBSAN). The latter phenomenon is the subject of this paper. It may be a strong source of disturbances at specific operating conditions. BBSAN was extensively studied experimentally by Norum and Seiner [9, 10] and more recently by André et al. [1, 2]. Numerically, De Cacqueray et al. [4] have used LES calculations for direct predictions. This valuable approach is time-consuming and not yet suitable for industrial needs.

The objective of this work is to develop a semi-analytical model, applicable to industrial geometries with reasonable computation time. The flight effect due to the flow surrounding the engine in real flight conditions is also taken into account.

The paper is organized as follows: first, the analytical derivation of the model is presented. The numerical implementation of the model is detailed in §3. Refraction effects are discussed in §4. Results are presented in §5.

2 BBSAN prediction

BBSAN is produced by the interaction of large-scale turbulent eddies and the quasi-periodic shock-cell structure of a shocked jet. Prediction methods rely on this physical principle, as proposed by Harper Bourne & Fisher [5] and Tam [15, 12]. They are suited for single-stream geometry but do not take the nozzle geometry into account. A more general approach is the following: compute the stationary turbulent flow field exiting from the nozzle, then extract the BBSAN sources from the aerodynamic field and eventually propagate the sound in the far-field. Morris & Miller used this technique [8, 6, 7]. The present work shares a common basis with Morris & Miller's model but bears some differences, outlined later on.

The Linearized Euler Equations (LEE) are written in terms of a dimensionless pressure variable $\pi = \frac{1}{\gamma}\ln(p/p_\infty)$, where γ is the specific heat ratio, p is the static pressure and p_∞ is the ambient pressure. The pressure and velocity field are split up into four components. For the pressure variable

$$\pi = \overline{\pi} + \pi_s + \pi_t + \pi' \tag{1}$$

The overline denotes the average field, the subscripts s and t the shock and turbulent perturbations, the superscript $'$ the acoustic perturbation generated by the interaction of shock-cells and turbulence. Keeping only the first-order interaction terms between shock and turbulence leads to

$$\frac{\partial \pi'}{\partial t} + \bar{v}_j \frac{\partial \pi'}{\partial x_j} + \frac{\partial v_i'}{\partial x_i} = 0 \tag{2}$$

$$\frac{\partial v_i'}{\partial t} + \bar{v}_j \frac{\partial v_i'}{\partial x_j} + v_j' \frac{\partial \bar{v}_i}{\partial x_j} + c_\infty^2 \frac{\partial \pi'}{\partial x_i} = f_i \tag{3}$$

where c_∞ is the ambient sound speed, v_i $(1 \le i \le 3)$ is the velocity field and f_i $(1 \le i \le 3)$ is the BBSAN source term, explicitly defined as

$$f_i = -v_{sj}\frac{\partial v_{ti}}{\partial x_j} - v_{tj}\frac{\partial v_{si}}{\partial x_j} \tag{4}$$

The other source terms, such as turbulent mixing noise, are not considered here. The system being linear, it will be solved using the Green function technique. Computing the Green's functions associated with (3) is cumbersome as shown by Morris & Miller [7]. The medium is assumed at rest ($\bar{v}_j = 0$) and refraction effects will be introduced later on. The Green's functions $\{\Pi_n, V_{ni}\}$ $(0 \le n \le 4)$ satisfy

$$\frac{\partial \Pi_n}{\partial t} + \frac{\partial V_{ni}}{\partial x_i} = \delta(\boldsymbol{x}-\boldsymbol{y})\delta(t-t_1)\delta_{0n}, 1 \le i \le 3 \tag{5}$$

$$\frac{\partial V_{ni}}{\partial t} + \bar{c}_\infty^2 \frac{\partial \Pi_n}{\partial x_i} = \delta(\boldsymbol{x}-\boldsymbol{y})\delta(t-t_1)\delta_{in} \tag{6}$$

It is then straightforward to determine π'

$$\pi'(\boldsymbol{x},t) = \int_{-\infty}^{+\infty}\int_{-\infty}^{+\infty} \Pi_n(\boldsymbol{x},\boldsymbol{y},t-t_1) f_n(\boldsymbol{y},t_1) d\boldsymbol{y} dt_1 \tag{7}$$

The solution to (5)-(6) writes

$$\Pi_n(\boldsymbol{x},\boldsymbol{y},\omega) \simeq -\frac{e^{-i\omega|\boldsymbol{x}-\boldsymbol{y}|/c_\infty}}{4\pi c_\infty^3}\frac{i\omega x_n}{|\boldsymbol{x}|^2} \tag{8}$$

in the far-field. The Power Spectrum Density is the Fourier transform of the correlation function, given by

$$\begin{aligned} S_{pp}(\boldsymbol{x},\omega) =& 2\pi(\rho_\infty c_\infty^2)^2 \int \dots \int \Pi_n(\boldsymbol{x},\boldsymbol{y_1},-\omega) \times \dots \\ & \Pi_m^*(\boldsymbol{x},\boldsymbol{y_1}+\boldsymbol{\eta},-\omega) R_{nm}(\boldsymbol{y_1},\boldsymbol{\eta},\tau) e^{-i\omega\tau} d\boldsymbol{y_1} d\boldsymbol{\eta} d\tau \end{aligned} \tag{9}$$

where $R_{nm}(\boldsymbol{y_1},\boldsymbol{\eta},\tau) = < f_n(\boldsymbol{y}_1,t_1) f_m(\boldsymbol{y}_1+\boldsymbol{\eta},t_1+\tau) >$ is the correlation between source terms and $< >$ is the ensemble average. The same assumptions as in Morris & Miller is made for the derivation of the source terms: the $f_n(\boldsymbol{y_1},t)$ $(1 \le n \le 3)$ terms are isotropic and using dimensional considerations

$$f_n(\boldsymbol{y_1},t) = f(\boldsymbol{y_1},t) = \frac{p_s(\boldsymbol{y_1}) v_t(\boldsymbol{y_1},t)}{\rho_\infty c_\infty l(\boldsymbol{y_1})} \tag{10}$$

where $v_t(\boldsymbol{y_1},t)$ is the characteristic turbulent velocity fluctuation and $l(\boldsymbol{y_1})$ is the characteristic turbulent length scale in the streamwise direction. Recasting this expression into the correlation term, it yields

$$R_{nm}(\boldsymbol{y_1},\boldsymbol{\eta},\tau) = \frac{p_s(\boldsymbol{y_1}) p_s(\boldsymbol{y_1}+\boldsymbol{\eta})}{\rho_\infty^2 c_\infty^2 l(\boldsymbol{y_1})^2} R_v(\boldsymbol{y_1},\boldsymbol{\eta},\tau) \tag{11}$$

where $R_v(\boldsymbol{y_1}, \boldsymbol{\eta}, \tau)$ is the correlation of turbulent velocity fluctuations. Following Tam's assumption [14], $R_v(\boldsymbol{y_1}, \boldsymbol{\eta}, \tau)$ is then modeled as

$$R_v(\boldsymbol{y_1}, \boldsymbol{\eta}, \tau) = k_t \exp[-|\tau|/\tau_s] \exp[-(\xi - u_c\tau)^2/l^2] \times ... \\ \exp[-(\eta^2 + \zeta^2)/l_\perp^2] \quad (12)$$

k_t is the turbulent kinetic energy, u_c is the eddy convection velocity, $l_\perp$ is the characteristic turbulent length scale in the cross-stream direction, τ_s is the turbulent time scale and $\boldsymbol{\eta} = (\xi, \gamma, \zeta)$. The last element required for the evaluation of S_{pp} is the Green's function $\Pi_m^*(\boldsymbol{x}, \boldsymbol{y_1} + \boldsymbol{\eta}, -\omega)$. In the geometric far-field, for $|\boldsymbol{x}| >> |\boldsymbol{y}|$

$$\Pi_m^*(\boldsymbol{x}, \boldsymbol{y_1} + \boldsymbol{\eta}, -\omega) = \Pi_m^*(\boldsymbol{x}, \boldsymbol{y_1}, -\omega) \exp\left[i\frac{\omega}{c_\infty}\frac{\boldsymbol{x}.\boldsymbol{\eta}}{|\boldsymbol{x} - \boldsymbol{y_1}|}\right] \quad (13)$$

The final expression for the PSD writes

$$S_{pp}(\boldsymbol{x}, \omega) = \frac{\omega^2}{8\pi c_\infty^4}\frac{1}{R^2}\int ... \int \frac{K(\boldsymbol{y})}{l(\boldsymbol{y})^2}\, p_s(\boldsymbol{y}) p_s(\boldsymbol{y} + \boldsymbol{\eta}) \times ... \\ \exp\left[-\frac{|\tau|}{\tau_s} - \frac{(\xi - u_c\tau)^2}{l^2} - \frac{\gamma^2 + \zeta^2}{l_\perp^2}\right] \times ... \\ \exp\left[i\omega\left(\frac{1}{c_\infty}\frac{\boldsymbol{x}.\boldsymbol{\eta}}{R} - \tau\right)\right] d\tau d\boldsymbol{\eta} d\boldsymbol{y} \quad (14)$$

where $R = |\boldsymbol{x}|$.

3 Numerical implementation

All the variables in (14) must be determined from a Reynolds-Averaged Navier-Stokes (RANS) solution. The perturbation due to shock-cells is evaluated by $p_s = p - p_a$ where p is the computed static pressure and p_a is the ambient pressure. The length scales are estimated by $l = c_l K^{3/2}/\varepsilon$, $l_\perp = c_\perp l$, while the time scale is assessed by $\tau_s = c_\tau K/\varepsilon$. The constants c_τ, c_l and $c_\perp$ are comparable to those in Tam's model and are set to $c_\tau = 0.49$, $c_l = 0.678$, $c_\perp = 0.17$.

For the computation of the PSD, Morris & Miller introduce the spatial Fourier transform of the pressure field in the axial direction, computed on a regular grid mesh. For academic geometries, this results in an easier numerical implementation of the model. Computing the Fourier transform may however be complex on industrial designs: the mesh used for the CFD computation is usually multi-block and the mesh lines are not always parallel to the x-axis, especially for nozzles with a plug in the primary stream, which is very common for dual-stream engines.

For these reasons, (14) is directly evaluated. Spatial integration along $\boldsymbol{y}$ and $\boldsymbol{\eta}$ should be carried out over the sources region only. Then, the specific implementation makes it possible to exclude useless blocks from the computation. Sound sources are expected to be located in regions of high turbulence intensity. All the cells that do not match this criterium are excluded from the integral. Correlation between sources remains significant over a limited distance, that is why a filter operates while integrating on $\boldsymbol{\eta} = (\xi, \gamma, \zeta)$: if $(\zeta^2+\gamma^2)/l_\perp^2 > 5$, then the current iteration is skipped.

For a given observer location and frequency, the computation basically consists in the evaluation of 7 nested loops. The integration over τ is the inner-most one. It is also the most difficult to compute. One has to evaluate

$$I(\omega) = \int_{-\infty}^{+\infty} g(\tau) \exp(-i\omega\tau) d\tau \quad (15)$$

where $g(\tau) = \exp\left[-\frac{|\tau|}{\tau_s} - \frac{(\xi - u_c\tau)^2}{l^2}\right]$, which boils down to compute the Fourier transform of g. $g(\tau)$ has a Gaussian shape with fast decay around its peak. The peak location is a function of ξ, u_c, τ_s, l and hence depends on the location in the flow. Calling τ_p the peak location of g, one has to distinguish among four cases

$$\begin{cases} \tau_p = \frac{1}{u_c}\left(\xi - \frac{l^2}{2u_c\tau_s}\right) & \text{for } \xi > 0 \text{ and } 2u_c\xi\tau_s - l^2 > 0 \\ \tau_p = 0 & \text{for } \xi > 0 \text{ and } 2u_c\xi\tau_s - l^2 < 0 \\ \tau_p = 0 & \text{for } \xi < 0 \text{ and } 2u_c\xi\tau_s + l^2 > 0 \\ \tau_p = \frac{1}{u_c}\left(\xi - \frac{l^2}{2u_c\tau_s}\right) & \text{for } \xi < 0 \text{ and } 2u_c\xi\tau_s + l^2 < 0 \end{cases} \quad (16)$$

Then $g(\tau)$ is sampled with about 200 points between $[\tau_p - 5l/u_c, \tau_p + 5l/u_c]$. To achieve sufficient frequency resolution, zero-padding is used before applying the FFT algorithm to the sampled signal.

4 Refraction effects

In the derivation of the model, the free-field Green's functions have been used, hence neglecting the possible refraction effects due to the mean flow. When comparing the model results to experiments, potential refraction effects should be considered.

On a single-stream jet, typical of an academic design, the sources of BBSAN are located in the shear-layer between the jet and the ambient (quiescent) medium. These sources will directly radiate into the free-field, therefore neglecting refraction is a reasonable assumption.

On a civil aircraft operating at cruise conditions, the primary flow is subsonic while the secondary flow is a supersonic shock-containing flow. There are two locations for the BBSAN sources: the shear-layer between the primary and secondary streams and the shear-layer between the secondary stream and the external flow. The waves originating from the former source are refracted when crossing the secondary shocked-stream and then the external shear-layer. The waves created in the outer shear-layer may be refracted by the external flow. In this case, neglecting refraction will lead to a mismatch in directivity estimation.

In the present work, a ray-tracing method is used to get an estimate of refraction effects. The ray-tracing basics are recalled and then the coupling process with the BBSAN model is presented.

4.1 The ray-tracing method

The ray-tracing approach provides a high-frequency solution to the LEE. It is similar to a multiple scale resolution of the LEE. Physically, the acoustic waves are locally described as plane waves. Ray paths are tangent to the group velocity and describe the propagation of acoustic energy. The ray paths are obtained by solving the eikonal equations

$$\begin{cases} \frac{dx_i}{dt} = c_0\frac{k_i}{k} + u_{0i} \equiv g_i(\boldsymbol{x}, \boldsymbol{k}), \ 1 \le i \le 3 \\ \frac{dk_i}{dt} = -k\frac{\partial c_0}{\partial x_i} - k_j\frac{\partial u_{0j}}{\partial x_i} \equiv h_i(\boldsymbol{x}, \boldsymbol{k}) \end{cases} \quad (17)$$

where $\boldsymbol{x}$ is the ray trajectory, $\boldsymbol{k}$ is the wave vector and $\boldsymbol{u_0}$ is the local velocity vector. The initial conditions are the source location and the shooting angles (θ_0, α_0) as defined in Figure 1. The acoustic flux is conserved in a ray tube

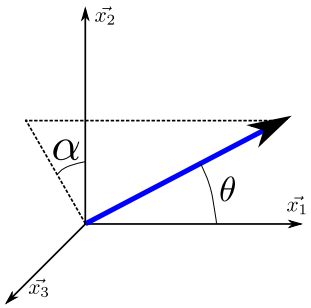

Figure 1: Coordinate system used for ray-tracing. x_1 is the jet axis.

$$\int_S E\boldsymbol{v_g}.\boldsymbol{n}dS = 0 \tag{18}$$

where E is acoustic energy density ($J.m^{-3}$), dS is the elementary surface of the ray tube cross-section, $\boldsymbol{n}$ is the normal vector to dS and $\boldsymbol{v_g}$ is the group velocity vector. The local interpretation of (18) is

$$E\boldsymbol{v_g} \cdot \boldsymbol{n}dS = \boldsymbol{I} \cdot \boldsymbol{n}dS = K_1 \tag{19}$$

where $\boldsymbol{I}$ is the acoustic intensity vector and K_1 is a constant equal to the acoustic power injected by the source in the ray tube. In the specific case of an isotropically radiating source

$$K_1 = \frac{d\Omega}{4\pi} W_a \tag{20}$$

where $d\Omega$ is the solid angle associated with the ray tube and W_a is the source power. $\boldsymbol{I}$ being colinear to the ray paths

$$I = \frac{K_1}{dS} \tag{21}$$

To track the evolution of dS along the ray paths, Candel [3] introduced the geodesic elements

$$\begin{cases} \boldsymbol{R}^\theta = \left(\dfrac{\partial \boldsymbol{x}}{\partial \theta_0}\right)_{t,\alpha_0} & \boldsymbol{R}^\alpha = \left(\dfrac{\partial \boldsymbol{x}}{\partial \alpha_0}\right)_{t,\theta_0} \\ \boldsymbol{Q}^\theta = \left(\dfrac{\partial \boldsymbol{k}}{\partial \theta_0}\right)_{t,\alpha_0} & \boldsymbol{Q}^\alpha = \left(\dfrac{\partial \boldsymbol{k}}{\partial \alpha_0}\right)_{t,\theta_0} \end{cases} \tag{22}$$

$\boldsymbol{R^\theta}$ quantifies the change in the ray path when slightly changing the shooting angle θ_0, the other variables being equal. The evolution of the geodesic elements is linked to the ray trajectory and wave vector by

$$\begin{cases} \dfrac{d\boldsymbol{R}}{dt} = \dfrac{\partial \boldsymbol{g}}{\partial \boldsymbol{x}}.\boldsymbol{R} + \dfrac{\partial \boldsymbol{g}}{\partial \boldsymbol{k}}.\boldsymbol{Q} \\ \dfrac{d\boldsymbol{Q}}{dt} = \dfrac{\partial \boldsymbol{h}}{\partial \boldsymbol{x}}.\boldsymbol{R} + \dfrac{\partial \boldsymbol{h}}{\partial \boldsymbol{k}}.\boldsymbol{Q} \end{cases} \tag{23}$$

After solving (23), the divergence or convergence of the rays is easily evaluated by

$$dS = |(d\theta_0 \boldsymbol{R}^\theta) \times (d\alpha_0 \boldsymbol{R}^\alpha) \cos(\boldsymbol{k}, \boldsymbol{v_g})| \tag{24}$$

and I is now fully determined by (21).

4.2 Coupling with the BBSAN model

The coupling technique between the BBSAN model and the ray-tracing method is presently under development. Considering acoustic sources distributed over volume V radiating into free-field, the acoustic pressure at location $\boldsymbol{x}$ and time t is given by

$$p'(\boldsymbol{x}, t) = \frac{1}{4\pi} \int_V S\left(\boldsymbol{y_1}, t - \frac{R_1}{c_\infty}\right) \frac{d\boldsymbol{y_1}}{R_1} \tag{25}$$

where $R_1 = |\boldsymbol{x} - \boldsymbol{y_1}|$ is the source-observer distance. Furthermore, the PSD of these sources is given by

$$\begin{aligned} S_{pp}(\boldsymbol{x}, t) = \frac{1}{16\pi^2} \iiint < S\left(\boldsymbol{y_1}, t - \frac{R_1}{c_\infty}\right) \times ... \\ S\left(\boldsymbol{y_2}, t + \tau - \frac{R_2}{c_\infty}\right) > \frac{1}{R_1 R_2} e^{-i\omega\tau} d\boldsymbol{y_1} d\boldsymbol{y_2} d\tau \end{aligned} \tag{26}$$

Figure 2 shows two elementary sources of sound located at $\boldsymbol{y_1}$ and $\boldsymbol{y_2}$. In a quiescent medium, the observer is located at $\boldsymbol{x}$. Radiation to the observer follows the straight lines (acoustic rays). The amplitude decays like $1/R_1R_2$ and the phase factor is $\tau - (R_2 - R_1)/c_\infty$.

In the presence of a mean flow, the ray shot from $\boldsymbol{y_1}$ to $\boldsymbol{x}$ is bent backwards and reaches $\boldsymbol{x'}$ instead, and so does the ray shot from $\boldsymbol{y_2}$. This results in a change in both phase and amplitude factors which can be evaluated with the ray-tracing method: the phase factor is obtained using the ray (bent) trajectories and the amplitude decay factor is provided by (21). Indeed, (21) relates the acoustic intensity anywhere on the ray to the power injected by the source in the tube. The transmission ratio between the source at $\boldsymbol{y_1}$ and the observer at $\boldsymbol{x'}$ is introduced

$$TL(\boldsymbol{y_1}, \boldsymbol{x'}) = 10 \log_{10}\left(\frac{I(\boldsymbol{x'})}{K_1}\right) \tag{27}$$

It remains to correctly link this ratio to account for refraction effects. The idea is here to consider each cell of the mesh as an acoustic source, the power of which will be damped by this transmission ratio before integration.

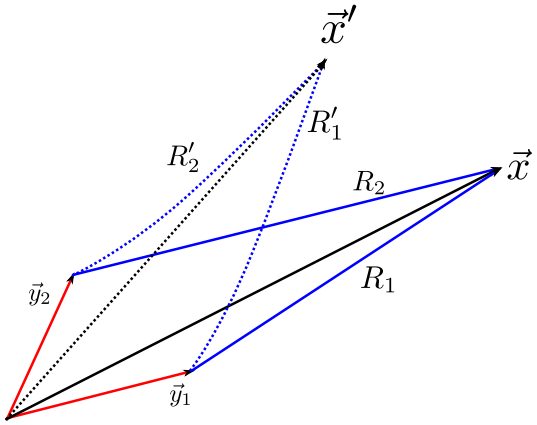

Figure 2: Illustration of the refraction effect on the ray paths. The dotted lines represent the refracted rays.

5 Results

Validation tests have been run on the ray-tracing algorithm. They include a dipole source with and without mean flow as well as a monopole source into an analytic jet velocity field.

The prediction capabilities of the BBSAN model have been assessed using experimental data by André and Castelain on both single-stream and dual-stream nozzles [1, 2]. The case of a convergent nozzle is described hereafter.

The jet isentropic Mach number is $M_j = 1.35$. The mean flow is computed using the elsA aerodynamic solver [11]. A Roe numerical scheme is coupled to a $k-\omega-SST$ turbulence model. The velocity field is shown in Figure 3. The shock-cell structure is clearly outlined as well as the shear-layer.

The ray-tracing algorithm is tested on this simple case by placing a monopole source inside the jet. The ray trajectories are shown in black lines in Figure 3. Rays are shot over the range $50° - 150°$ (downstream reference). The rays do not propagate in the upstream supersonic regions, this confirms that acoustic perturbations cannot sail the supersonic flow up. The rays are bent towards the lower velocity region as expected.

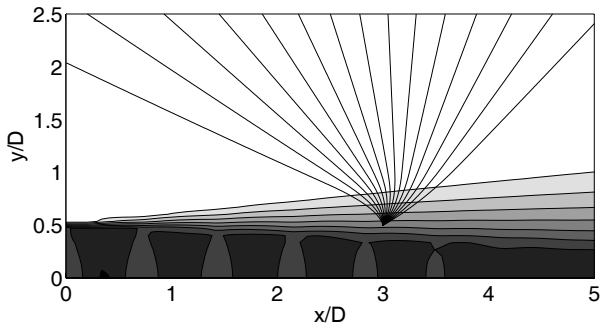

Figure 3: Ray-tracing algorithm for a source located in a shocked jet, $M_j = 1.35$. The velocity field is shown, the color scale ranges for levels from 0 to 400 m/s, from white to gray. The ray paths are shown in straight lines.

The results presented in Figure 4 show the PSDs for a convergent jet at an isentropic Mach $M_j = 1.35$. Different angles are presented using a downstream reference. The typical features of the BBSAN are correctly captured by the model: the humps of the BBSAN are well located for the different angles. The peak frequency increases from the forward to the backward direction as expected. On the measured data, strong screech peaks spring and should not be considered when evaluating the BBSAN prediction capabilities of the model. The model overestimates the sound levels at high frequency. Interpretations and inclusion of refraction effects are currently under investigation.

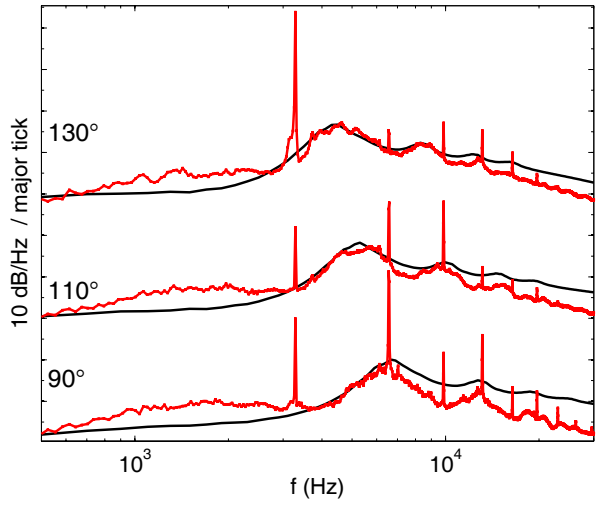

Figure 4: PSDs for a convergent jet at $M_j = 1.35$ at different angles (downstream reference). —— : measurements by B. André and T. Castelain [1]. —— : calculations.

6 Conclusion

The model presented in this paper is aimed at predicting BBSAN including propagation effects. It uses a RANS solution of the jet flow field and a ray-tracing algorithm to account for refraction effects.

For time being, results are only available for single-stream jets, without refraction effects. The example given on a $M_j = 1.35$ jet showed very encouraging results. Dual-stream calculations have been made and the model will be tested on these more realistic geometries soon.

The ray-tracing algorithm is functional, provides consistent results for simple test cases and its coupling with the BBSAN model is being examined. Assessment of refraction effects through this approach should be available soon.

When the coupling is done, extensive comparisons with measurements will be performed. This includes dual-stream jets at different Mach numbers, in static and flight conditions.

Possible improvements include running an optimization step to determine the best constants in the correlation function. The use of an adjoint approach (see [13]) for the ray-tracing problem is also under examination. It could lead to great savings in computation times.

References

[1] B. André, T. Castelain, and C. Bailly. Experimental exploration of an underexpanded supersonic jet. In *28th International Symposium on Shock Waves*, number 1, Manchester, 2011.

[2] B. André, T. Castelain, and C. Bailly. Experimental study of flight effects on screech in underexpanded jets. *Physics of Fluids*, 23(12):1–14, 2011.

[3] S. Candel. Numerical solution of conservation equations arising in linear wave theory: application to aeroacoustics. *Journal of Fluid Mechanics*, 83:466–493, 1977.

[4] N. de Cacqueray, C. Bogey, and C. Bailly. Investigation of a high-Mach-number overexpanded jet using Large-Eddy Simulation. *AIAA Journal*, 49(10), 2011.

[5] M. Harper-Bourne and M.J. Fisher. The noise from shock waves in supersonic jets. In *AGARD Noise Mech. 13 p (SEE N74-22640 14-02); International Organization*, 1973.

[6] S.A.E Miller and P.J. Morris. The prediction of broadband shock-associated noise from dualstream and rectangular jets using RANS CFD. In *16th AIAA/CEAS Aeroacoustics Conference*, 2010.

[7] S.A.E Miller and P.J. Morris. The prediction of broadband shock-associated noise including propagation effects. In *17th AIAA/CEAS Aeroacoustics Conference*, number June, pages 05 – 08, 2011.

[8] P.J. Morris and S.A.E Miller. The prediction of broadband shock-associated noise using RANS CFD. In *15th AIAA Aeroacoustics Conference*, 2009.

[9] T.D. Norum and J.M. Seiner. Broadband shock noise from supersonic jets. *AIAA Journal*, 20(1):68–73, 1982.

[10] T.D. Norum and J.M. Seiner. Measurements of mean static pressure and far-field acoustics of shock-containing supersonic jets. *NASA Technical Memorandum - 84521*, 1982.

[11] ONERA. elsA Aerodynamics Simulation Software Package.

[12] C.K.W. Tam. Stochastic model theory of broadband shock associated noise from supersonic jets. *Journal of Sound and Vibration*, 116:265–302, 1987.

[13] C.K.W. Tam and L. Auriault. Mean flow refraction effects on sound radiated from localized sources in a jet. *Journal of Fluid Mechanics*, 370:149–174, 1998.

[14] C.K.W. Tam and L. Auriault. Jet mixing noise from fine-scale turbulence. *AIAA Journal*, 37(2):145–153, 1999.

[15] C.K.W. Tam and H.K. Tanna. Shock associated noise of supersonic jets from convergent-divergent nozzles. *Journal of Sound and Vibration*, 81:337–358, 1982.